Article

Journal of
Nanoscience and Nanotechnology
Vol. 15, 8667–8673, 2015
www.aspbs.com/jnn

Effect of Embedded RF Pulsing for Selective Etching of SiO_2 in the Dual-Frequency Capacitive Coupled Plasmas

Nam Hun Kim[1,2], Min Hwan Jeon[3], Tae Hyung Kim[4], and Geun Young Yeom[3,4,*]

[1] Giheung Hwasung Complex, Semiconductor Business, Samsung Electronics, Banwol-Dong, Hwasung-City, Gyeonggi-Do 445-982, South Korea
[2] College of Information and Communication Engineering, Sungkyunkwan University, Suwon, Gyeonggi-do 440-746, South Korea
[3] SKKU Advanced Institute of Nano Technology (SAINT), Sungkyunkwan University, Suwon, Gyeonggi-do 440-746, South Korea
[4] Department of Advanced Materials Science and Engineering, Sungkyunkwan University, Suwon, Gyeonggi-do 440-746, South Korea

The characteristics of embedded pulse plasma using 60 MHz radio frequency as the source power and 2 MHz radio frequency as the bias power were investigated for the etching of SiO_2 masked with an amorphous carbon layer (ACL) using an $Ar/C_4F_8/O_2$ gas mixture. Especially, the effects of the different pulse duty ratio of the embedded dual-frequency pulsing between source power and bias power on the characteristics on the plasma and SiO_2 etching were investigated. The experiment was conducted by varying the source duty percentage from 90 to 30% while bias duty percentage was fixed at 50%. Among the different duty ratios, the source duty percentage of 60% with the bias duty percentage of 50% exhibited the best results in terms of etch profile and etch selectivity. The change of the etch characteristics by varying the duty ratios between the source power and bias power was believed to be related to the different characteristics of gas dissociation, fluorocarbon passivation, and ion bombardment observed during the different source/bias pulse on/off combinations. In addition, the instantaneous high electron temperature peak observed during each initiation of the source pulse-on period appeared to affect the etch characteristics by significant gas dissociation. The optimum point for the SiO_2 etching with the source/bias pulsed dual-frequency capacitively coupled plasma system was obtained by avoiding this instant high electron temperature peak while both the source power and bias power were pulsed almost together, therefore, by an embedded RF pulsing.

Keywords: Embedded Pulse Plasma, Pulsed Dual Frequency CCP, SiO_2 Etching, Duty Ratio.

1. INTRODUCTION

In the fabrication of nano devices, the pattern size has gradually been reduced to the deep nano scale for the better performance and ultra large scale integration (ULSI).[1–3] As a result, the lateral dimension of the devices was reduced significantly to tens of nanometers; however, the vertical dimension of the devices could not be decreased proportionally to maintain the device properties. Therefore, the aspect ratio of the devices has been significantly increased and one of the important processes for ULSI devices is the dry etching process for the high aspect ratio contact (HARC).[4–7] For the HARC etching, there are several challenges such as higher etch selectivity, tighter critical dimensional control, and lower plasma induced damage caused by the incident high ion bombardment energy.[8–13]

To overcome those challenges, therefore, for nano-scaled selective etching with low damage, the various plasma etching methods have been widely investigated.[14–19] The pulsed plasma etching is one of the most promising candidates for improvement of the etch characteristics in the etching of nano-scaled materials. It is possible to control the plasma characteristics such as plasma chemical composition and ion bombardment

*Author to whom correspondence should be addressed.

energy independently and additionally by adjusting the pulse parameters such as duty ratio and pulse frequency during the operation of the plasmas. The reported main advantages of pulsed plasma were reported to be improvement of the etch selectivity and etch uniformity due to the decreased gas dissociation and enhanced radical diffusion. In addition, control of the etch profile and critical dimension was reported due to the reduction of plasma-induced damage by charging. Thus, pulsed plasma technology has been widely investigated for nano-scaled etching applications to improve the plasma uniformity, etch selectivity, and etch profile by reducing the plasma-induced damages. Especially, dual-pulsed plasma etching using pulse synchronization is a strong candidate for obtaining deep nanoscale HARCs, wherein both the bias and source are simultaneously pulsed (synchronous pulsing) with or without time delay between them. Since the power is actively deposited for only a fraction of the time, pulsed plasmas offer the possibility of working with low electron energy regimes and with less dissociated (and less reactive) plasmas, resulting in better process performance in terms of damage, selectivity, and etch profile control.[20]

For nanoscale HARC etching with synchronous pulsing, the effects of the pulse parameters such as pulse frequency, phase lag between the source and bias pulses, etc., have been widely investigated.[21–25] However, the effects of other pulsing techniques such as changing the duty ratios between the source power and the bias power during HARC etching, have not yet been fully investigated, and thus require a more detailed examination. Therefore, in this study, an embedded radio frequency (RF) pulsing for dual-frequency capacitive coupled plasma (DF-CCP) was used, and the effects of different duty ratios between source pulsing and bias pulsing on the characteristics of the plasma and the HARC etching was studied.

2. EXPERIMENTAL DETAILS

The experimental setup of the embedded pulse DF-CCP system used in this study is shown in Figure 1. The radio frequency (RF) discharge was maintained between the two parallel plate electrodes, which were separated by 30 mm. The top electrode was covered with a perforated silicon plate to flow gases uniformly and it was connected to a 60 MHz RF power (high frequency; HF) source which could be pulsed to control the plasma characteristics and to control the pulse signal delay of the 2 MHz (low frequency; LF) pulsed RF power applied to the substrate. Synchronization of the 2 MHz RF power to the 60 MHz RF power was obtained by connecting the 60 MHz pulse signal to a digital delay generator (DDG 645, SRS), a signal generator (8657B, HP), and an RF power amplifier (A1000, ENI), in series. Therefore, the source power pulsing was served as a master and the bias power pulsing was served as a slave by receiving the source pulse signal from the DDG. The pulse signal generated from the

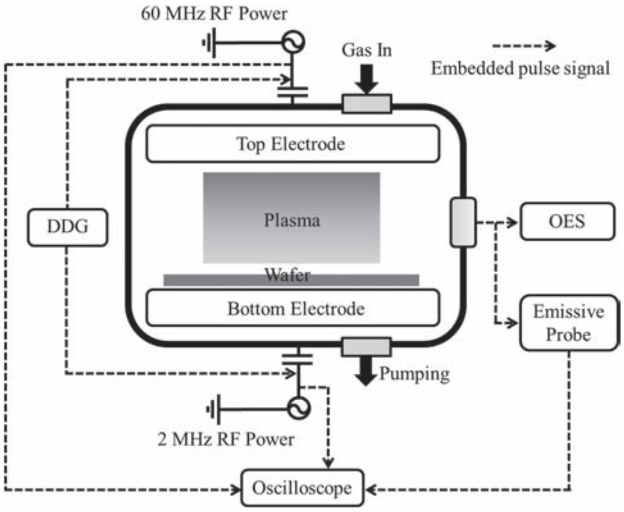

Figure 1. Schematic diagram of the embedded pulse dual-frequency CCP. A pulsed 60 MHz source pulse power was applied to the top electrode to control the plasma characteristics and a pulsed 2 MHz bias power was applied to the bottom electrode to control the ion energy to the substrate.

60 MHz was also used to control the time-resolved optical emission spectrometer (OES) installed on the quartz window. An emissive probe was installed inside the chamber to observe the temporal electron temperatures. Figure 2 shows a cartoon illustration of the embedded pulse waveform for the pulse duty ratios between te source hpower pulsing and bias power pulsing during the embedded pulsing of 60/2 MHz CCP. In addition to the 60 MHz source power, the 2 MHz bias power applied to the substrate was embeddedly pulsed with the source power. As shown in the figure, the duty percentage of the source power pulse was varied from 30 to 90% while keeping 50% of bias power pulsing. The bias pulse was set to be synchronously ended when the source pulse was ended.

The 2 μm thick SiO_2 deposited on silicon wafers was masked with a 600 nm thick amorphous carbon layer (ACL). The ACL was used as the hardmask for SiO_2 HARC etching to maintain the critical dimension (CD) of the contact hole. The SiO_2 layer was etched by various source duty percentages as shown in Figure 2 while keeping the bias both duty percentage at 50% and the pulse frequency at 1 KHz in the embedded pulsing. $Ar/C_4F_8/O_2$ gas chemistry (60 MHz HF power/2 MHz LF bias voltage = 300 W/−1000 V, $Ar/C_4F_8/O_2$ = 140/40/5 sccm, and the process pressure of 30 mTorr) was used while maintaining the substrate temperature at room temperature by water cooling. For various duty ratio conditions, the etching time was varied for about 1300 nm thickness of etch depth after dry etching.

Etch characteristics such as the etch rates of SiO_2 HARC layer/ACL and the etch profiles using the $Ar/C_4F_8/O_2$ gas chemistry were estimated by field emission scanning electron microscopy (FE-SEM, Hitachi

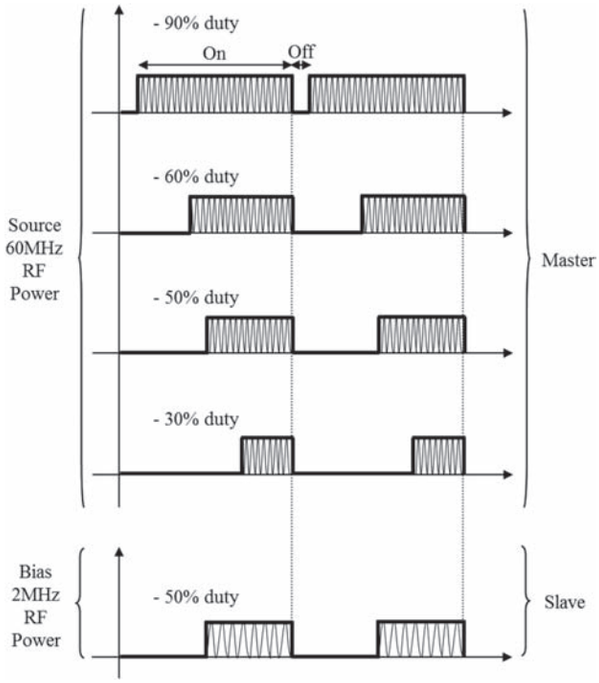

Figure 2. Schematic diagram of the pulse waveform between source power pulsing and bias power pulsing for various duty ratios in the embedded pulse 60/2 MHz CCP.

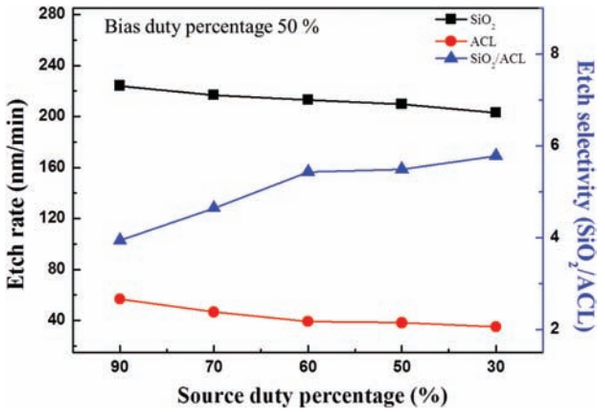

Figure 3. Etch rates of SiO_2 and ACL, and the etch selectivity of SiO_2/ACL measured as a function of the source pulse duty percentage while the bias duty percentage was kept at 50% and the pulse frequency at 1 kHz. The bias pulse was synchronously ended when the source pulse was ended. 300 W of 60 MHz RF power and −1000 V of 2 MHz RF bias voltage were used with the gas flow rates of Ar (140 sccm)/C_4F_8/(40 sccm) O_2 (5 sccm) and the operating pressure of 30 mTorr.

S-4700). The radicals which dominantly affect the etching were observed using time-resolved optical emission spectroscopy (OES). The time-resolved OES (Andor iStar 734) was composed of a grating monochromator and an intensified charge coupled device (ICCD). For the time-resolved data collection, the OES data were collected with the interval of 100 μs in the 1 kHz of pulse period and the data were averaged after the collection for 10 times. The instant change of the electron temperature for variously embedded pulse conditions of 60/2 MHz DF-CCP was calculated by using a home-made emissive probe. In addition, the chemical binding characteristics of the etched SiO_2 surface for the differently embedded pulse conditions were observed using X-ray photoelectron spectroscopy (XPS, ESCA2000, VG Microtech Inc.).

3. RESULTS AND DISCUSSION

Etch rates of SiO_2 and ACL, and the etch selectivity of SiO_2/ACL measured as a function of the source pulse duty percentage while the bias duty percentage was kept at 50% and the pulse frequency at 1 kHz and the results are shown in Figure 3. The bias pulse was synchronously ended when the source pulse was ended as shown in Figure 2. The conditions of 300 W of 60 MHz RF power and −1000 V of 2 MHz RF bias voltage were used with the gas flow rates of Ar (140 sccm)/C_4F_8 (40 sccm)/O_2 (5 sccm) and the operating pressure of 30 mTorr. As shown in the figure, with decrease of the source duty percentage from 90 to 30% while keeping the bias duty percentage at 50%, both the SiO_2 etch rate and ACL etch rate were decreased possibly indicating etching of the materials by reactive gas species dissociated by the source power only while no bias power was applied. Because the ACL layer was preferentially etched for the condition with the source power only, the etch selectivity was increased with the decrease of the source pulse percentage; however, it was almost saturated at the source power pulse percentage of 60%.

The SiO_2 etch profiles masked with an ACL for the conditions in Figure 3 were observed by FE-SEM and the results are shown in Figure 4. The thickness of the ACL was 600 nm and the etch depth of SiO_2 was kept at 1.3 μm. The etch rate of SiO_2 was decreased with decrease of the source duty percentage; therefore, longer etching time was required to etch SiO_2 to 1.3 μm deep for the lower duty percentages. As shown in the figure, as the source duty percentage was decreased from 90 to 60% while the bias duty percentage was fixed at 50%, more anisotropic etch profile was observed. In addition, the critical dimension (CD) of the contact hole was decreased with decreasing source duty percentage. However, when the source duty percentage was further decreased to 50% and 30% while keeping the bias duty percentage at 50%, the etch profile changed worse again by showing bow-like sidewall while remaining the similar ACL layer thickness.

To understand the results of the etch rates and etch profiles observed as a function of the source pulse duty percentages in Figures 3 and 4, changes of the time-varying plasma characteristics by the different pulse duty percentages were investigated using an emissive probe and time-resolved OES. Figure 5 shows the instant variation of electron temperature estimated as a function of time for the source pulse duty percentages of (a) 30%, (b) 50%, (c) 60% and (c) 90% while the bias duty

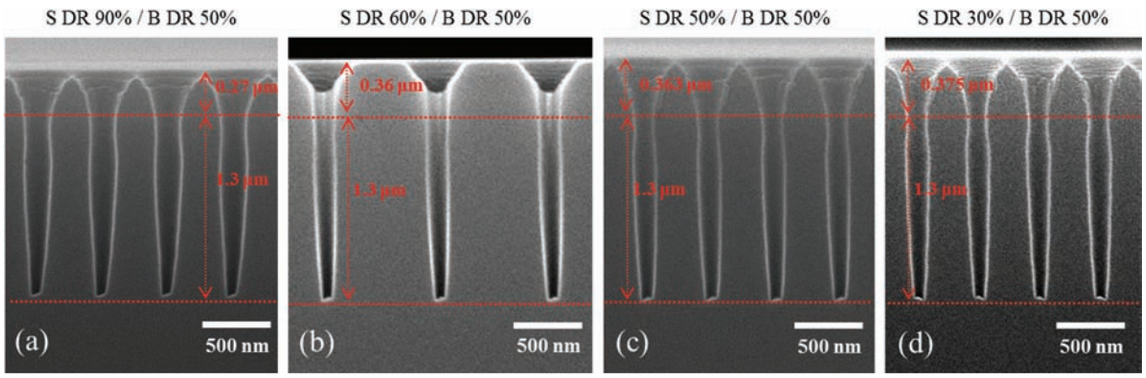

Figure 4. Etch profiles of ACL-masked SiO_2 contact hole pattern observed by FE-SEM after etching as a function of the embedded pulse duty cycle of (a) 90%, (b) 60%, (c) 50%, and (d) 30%, while the bias duty percentage was kept at 50% and the pulse frequency at 1 kHz. The etch time of SiO_2 contact hole was varied to obtain the etching depth of about 1.3 μm. The process conditions are the same as those in Figure 3.

percentage was kept at 50% and the pulse frequency of 1 kHz. The bias pulse was set to be synchronously ended when the source pulse was ended. 300 W of 60 MHz RF power and −1000 V of 2 MHz RF bias voltage were used with 140 sccm of Ar gas flow rate and 30 mTorr of operating pressure. By the emissive probe, the time-varying plasma potentials (V_p) and floating potentials (V_f) were measured and the instant electron temperature (T_e) was calculated from the following equation;

$$V_p - V_f = \frac{kT_e}{2e} \ln\left(\frac{2M}{\pi m}\right)$$

where, k is the Boltzmann constant, T_e is the electron temperature, m is the electron mass, and M is the Ar atomic

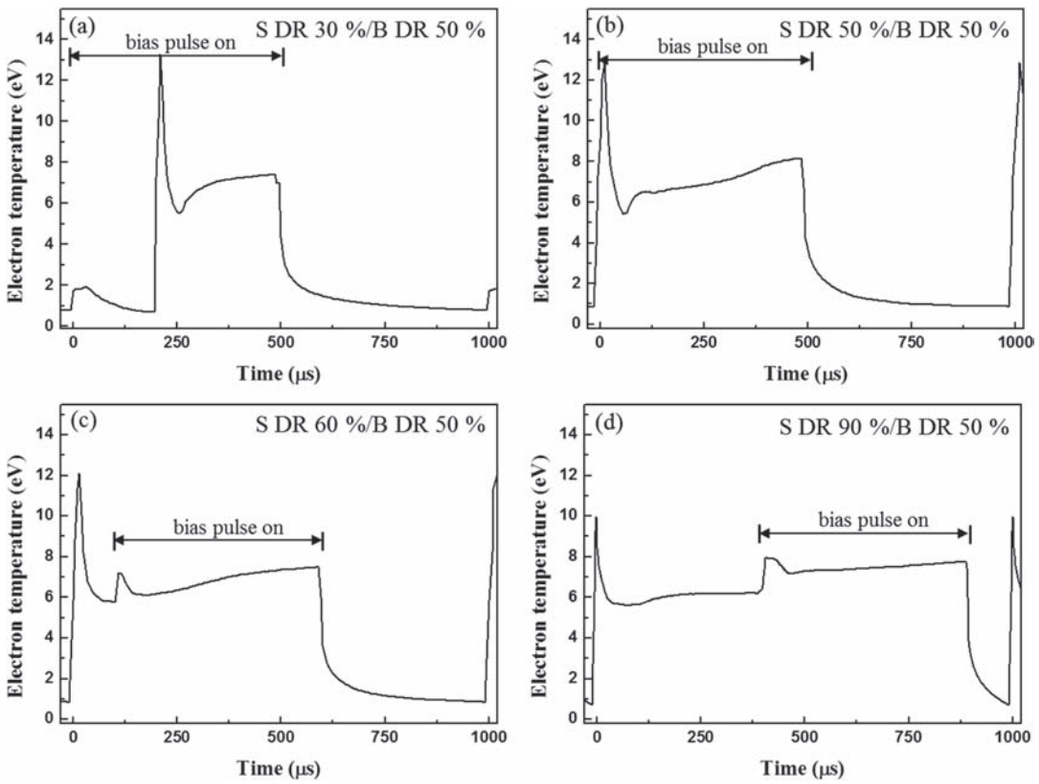

Figure 5. Instant variation of electron temperature estimated as a function of time for the source pulse duty percentages of (a) 30%, (b) 50%, (c) 60% and (c) 90%, while the bias duty percentage was kept at 50% and the pulse frequency at 1 kHz. The bias pulse was synchronously ended when the source pulse was ended. 300 W of 60 MHz RF power and −1000 V of 2 MHz RF bias voltage were used with the Ar gas flow rate of 140 sccm and the operating pressure of 30 mTorr.

mass. As shown in Figure 5, when the source pulse was initiated, a sudden increase of the electron temperature of about 10∼14 eV was observed and the electron temperature was rapidly decreased to about 6 eV and was slightly increased with time until the source pulse was off. For the bias pulsing, it also showed a slight increase of electron temperature during the initiation of the bias pulsing to about 2 eV and and the electron temperature was rapidly decreased to about 1 eV. Therefore, as shown in Figure 5, for the source pulse duty percentages of 30% and 50%, a high instant electron temperature peak was embedded in the bias pulse on time, while it was not embedded for the source pulse percentages of 60% and 90%.

To determine the effects of the different electron temperatures observed during the synchronized dual frequency pulsing on change of the gas dissociation characteristics, the temporal gas dissociation characteristics were measured using time-resolved OES. Figure 6 shows the time-resolved OES intensity ratios of F/Ar, CF_x/Ar ($x = 2, 3$), and CF_x/F ($x = 2, 3$) measured as a function of the source pulse duty percentage from 30 to 90%, while the bias pulse duty percentage was fixed at 50%. The process conditions were the same as those in Figure 4. As the OES peak intensities, the peak intensities observed at 703 nm, 245∼265 nm, 265∼285 nm, and 751 nm were used for F, CF_2, CF_3, and Ar, respectively, and the optical emission intensity ratios of the dissociated radicals to Ar were used for estimation of the radical concentration in the plasma. As shown, when the source pulse was on, radicals such as F, CF_2, and CF_3 were increased and low CF_x ($x = 2, 3$)/F ratios were obtained due to the increased gas dissociation caused by the high electron temperature of 6∼8 eV obtained with the high frequency source power shown in Figure 5, regardless of the low frequency bias pulse (on or off). Especially when the source pulse was initiated, due to the instant high electron temperature peak of 10∼14 eV, the higher radical concentrations and lower CF_x ($x = 2, 3$)/F ratios were observed by the higher gas dissociation. On the contrary, when the source pulse was off, regardless of the bias pulse (on or off), the radicals were decreased slowly due to recombination of the dissociated gases. In addition, when the source power was off, the CF_x ($x = 2, 3$)/F ratios were increased significantly indicating the possibility to form a high fluorocarbon passivation layer.

To investigate the possibility of formation of a fluorocarbon layer on the ACL and the sidewall of the etched SiO_2, the chemical binding characteristics of the etched

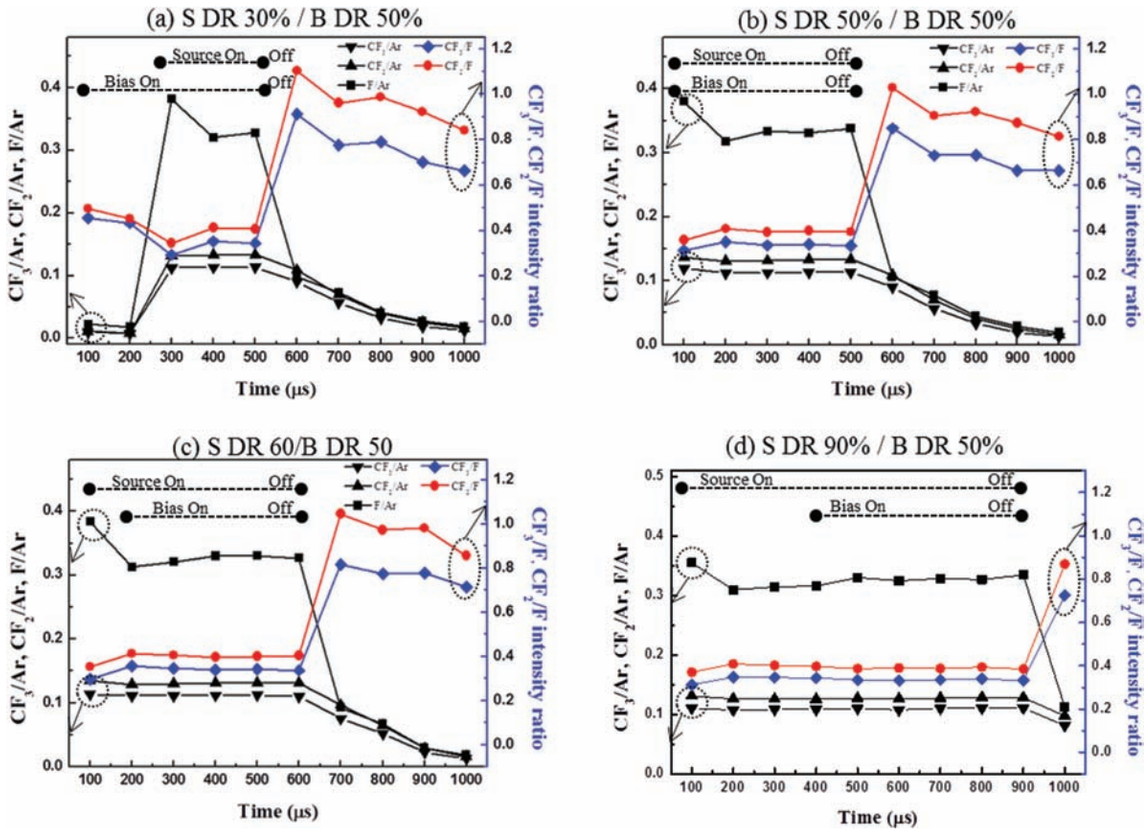

Figure 6. Time-resolved OES intensity ratios of F/Ar, CF_x/Ar ($x = 2, 3$), and CF_x/F ($x = 2, 3$) measured as a function of the source pulse duty percentage from 30 to 90% while the bias pulse duty percentage was fixed at 50%. The process conditions are the same as those in Figure 4. The source duty percentages: (a) 30%, (b) 50%, (c) 60%, and (d) 90%.

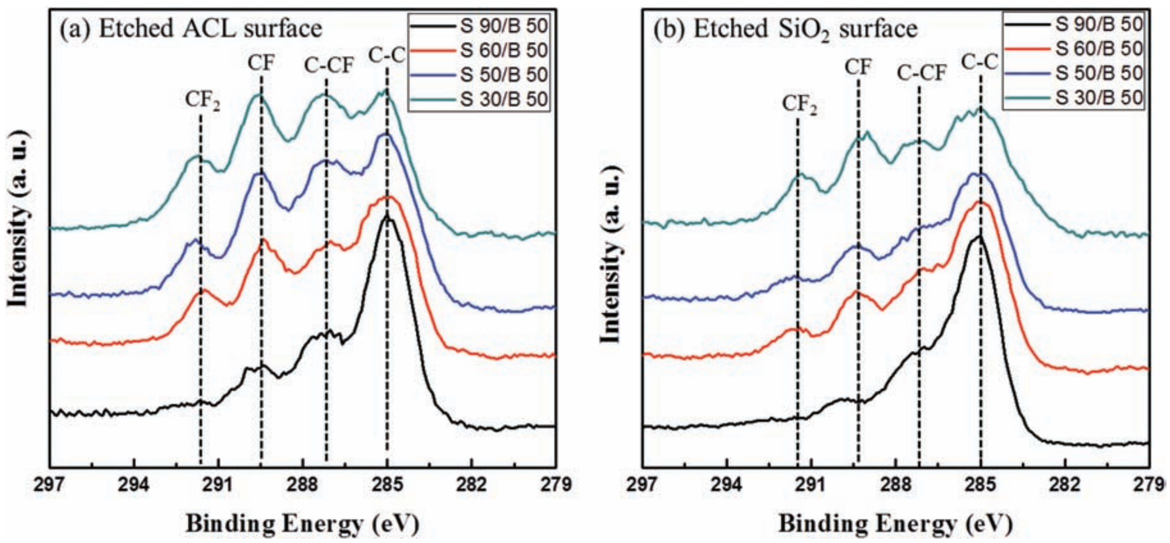

Figure 7. XPS narrow scan data of C1*s* of (a) the etched ACL surface and (b) the etched SiO_2 surface for different pulse duty percentages of 30∼90% while the bias duty percentage was kept at 50%. The SiO_2 and ACL were etched until 1.3 μm of SiO_2 was etched. The process conditions are the same as those in Figure 4.

SiO_2 surface and ACL surface were investigated using XPS. Figures 7(a) and (b) show the results of carbon binding states for the etched ACL surface and etched SiO_2 surface measured for different pulse duty percentages, respectively. To analyze the carbon binding states (C1*s*), blank SiO_2 and ACL were etched until 1.3 μm of SiO_2 was etched with various duty percentages. The process conditions were the same as those in Figure 4. As the C1*s* binding peaks, peaks related to C–C (285.0 eV), C–CF (287.4 eV), CF (289.6 eV), and CF_2 (291.7 eV) could be observed. The CF_x ($x = 1$, 2) binding in the XPS C1*s* narrow scan data was related to the fluorocarbon polymer passivation layer formed on the material surfaces. As shown in the figure, a fluorocarbon passivation layer was formed both on the SiO_2 surface and on the ACL surface. In addition, the binding peak intensities related to CF and CF_2 were increased as the source duty percentage was decreased from 90 to 60%, possibly indicating increased thickness of the fluorocarbon passivation layer. However, further decrease of the source pulse duty percentage to 50 and 30% did not change the peak intensities related to CF and CF_2 significantly, indicating no significant change in the fluorocarbon layer thickness.

From Figures 5 to 7, the improvement of etch selectivity and etch profile observed in Figures 3 and 4, respectively, by decreasing the source pulse duty percentage from 90 to 60% are believed to be related to the increased thickness of the fluorocarbon passivation layer on the ACL mask surface and the sidewall of the etched SiO_2 surface. When the source pulse duty percentage is equal to and lower than 50%, the instant high electron temperature peak is included in the bias pulse on-time and the bias pulse stays on without the source power for the source duty percentage less than 50%. Therefore, the ACL mask is bombarded by energetic reactive ions and shows the enhanced edge erosion (facet). Mask faceting is a well-known event, generating the profile distortion during plasma processes. It is generated by sputtering the edge of the mask by high energy ions. Once it has been initiated, the facet develops very fast since the sputtering rate of non-horizontal surfaces (the edge of the mask) is higher than flat surfaces (the top of the mask). The faceting of the ACL mask increases the ion scattering to the sidewall of the SiO_2 contact hole, therefore, forms bow-like SiO_2 etch profiles as shown in Figures 4(c) and (d). Eventually, the most anisotropic SiO_2 etch profile observed in Figure 4(b) is believed to be obtained by avoiding the source pulse initiation period during the bias pulse on time while almost synchronously pulsing the source power and the bias power, that is, by using the embedded pulsing of 60% source pulsing with 50% bias pulsing.

4. CONCLUSION

The effects of the pulse duty ratio between the 60 MHz source power applied to the top electrode and the 2 MHz bias power applied to the bottom substrate during the dual pulsed 60/2 MHz CCP on the plasma characteristics and etch characteristics of SiO_2 were investigated using an $Ar/C_4F_8/O_2$ gas mixture. In all of conditions, regardless of the bias power pulsing, low CF_x/F ratios were observed during the source power pulse on time due to the high electron temperature of about 6∼8 eV. Especially, a lower CF_x/F ratio with a higher electron temperature peak of about 10∼14 eV was observed during the initiation period of the source pulse. However, when

the source pulse was off, regardless of the bias power pulsing, high CF_x/F ratios with electron temperatures of 1~2 eV were observed. As the source pulse duty percentage was decreased from 90 to 60% while the bias duty ratio was fixed at 50%, the etch selectivity of SiO_2/ACL was improved and the etch profile became more anisotropic. However, when the source pulse duty ratios were decreased further to 50 and 30%, the etch profile changed to bow-like sidewall etch profile while the etch selectivity was remaining similar. The improvements of the etch selectivity and etch profile observed by decreasing the source pulse duty percentage from 90 to 60% were believed to be related to the increased thickness of the fluorocarbon passivation layer, caused by high CF_x/F ratios during the source pulse off time. The bow-like etch profiles obtained for the source duty percentages of 50 and 30% were believed to be related to the involvement of initial high gas dissociation period during the initiation of the source pulse and the energetic reactive ion bombardment without the source pulse on. Therefore, the most anisotropic SiO_2 etch profile could be obtained by avoiding the source pulse initiation period during the bias pulse on time, while almost synchronously pulsing the source power and bias power, that is, by using the embedded pulsing of 60% source pulsing with 50% bias pulsing.

Acknowledgments: This work was supported by the Industrial Strategic Technology Development Program (10041681, Development of fundamental technology for 10 nm process semiconductor and 10 G size large area process with high plasma density and VHF condition), funded by the Ministry of Knowledge Economy (MKE, Korea). Support was also provided by the MOTIE (Ministry of Trade, Industry and Energy (10049065) and KSRC (Korea Semiconductor Research Consortium) support program which development of future semiconductor device and nano material technology development program through the National Research Foundation of Korea (NRF), funded by the Ministry of Education, Science and Technology (2012M3A7B4035323).

References and Notes

1. T. Skotnicki, et al., *IEEE Trans. Electron Devices* 55, 96 (**2008**).
2. R. F. Pease and S. Y. Chou, *Proc. IEEE* 96, 248 (**2008**).
3. S. Banna, A. Agarwal, G. Cunge, M. Darnon, E. Pargon, and O. Joubert, *J. Vac. Sci. Technol., A* 30, 040801 (**2012**).
4. D. Koehler and D. Fischer, *ECS Trans.* 138, 47 (**2008**).
5. H. Abe, M. Yoneda, and N. Fujiwara, *Jpn. J. Appl. Phys.* 47, 1435 (**2008**).
6. T. Goto, H. Yamauchi, T. Kato, M. Terasaki, A. Teramoto, M. Hirayama, S. Sugawa, and T. Ohmia, *Jpn. J. Appl. Phys., Part 1* 43, 1784 (**2004**).
7. M. Izawa, N. Negishi, K. Yokogawa, and Y. Momonoi, *Jpn. J. Appl. Phys. Part* 1 46, 7870 (**2007**).
8. D. Zhang and M. J. Kushner, *J. Vac. Sci. Technol., A* 19, 524 (**2001**).
9. T. Goto, K. Ikenaga, A. Teramoto, M. Hirayama, S. Sugawa, and T. Ohmi, *J. Vac. Sci. Technol., A* 26, 8 (**2008**).
10. K. Hashimoto, *Jpn. J. Appl. Phys.* 32, 6109 (**1993**).
11. K. Eriguchi and K. Ono, *J. Phys. D* 41, 024002 (**2008**).
12. D. Fuard, O. Joubert, L. Vallier, M. Assous, P. Berruyer, and R. Blanc, *J. Vac. Sci. Technol., B* 19, 2223 (**2001**).
13. G. S. Hwang and K. P. Giapis, *J. Vac. Sci. Technol., B* 15, 70 (**1997**).
14. S. Samukawa, *Appl. Phys. Lett.* 64, 3398 (**1994**).
15. T. Ohmori, T. K. Goto, T. Kitajima, and T. Makabe, *Jpn. J. Appl. Phys.* 44, L1105 (**2005**).
16. A. Yokozawa, H. Ohtake, and S. Samukawa, *Jpn. J. Appl. Phys.* 35, 2433 (**1996**).
17. H. Abe, M. Yoneda, and N. Fujiwara, *Jpn. J. Appl. Phys.* 47, 1435 (**2008**).
18. H. Ohtake, K. Noguchi, S. Samukawa, H. Iida, A. Sato, and X. Qian, *J. Vac. Sci. Technol., B* 18, 2495 (**2000**).
19. G. Cunge, D. Vempaire, R. Ramos, M. Touzeau, O. Joubert, P. Bodard, and N. Sadeghi, *Plasma Sources Sci. Technol.* 19, 034017 (**2010**).
20. L. Xu, D. J. Economou, V. M. Donnelly, and P. Ruchhoeft, *Appl. Phys. Lett.* 87, 041502 (**2005**).
21. H. Shin, W. Zhu, L. Xu, T. Ouk, D. J. Economou, and V. M. Donnelly, *Plasma Sources Sci. Technol.* 20, 055001 (**2011**).
22. M. D. Logue, H. Shin, W. Zhu, L. Xu, V. M. Donnelly, D. J. Economou, and M. J. Kushner, *Plasma Sources Sci. Technol.* 21, 065009 (**2012**).
23. K. Tokashiki, H. Cho, S. Banna, J. Y. Lee, K. Shin, V. Todorow, W. S. Kim, K. H. Bai, S. Joo, J. D. Choe, K. Ramaswamy, A. Agarwal, S. Rauf, K. Collins, S. J. Choi, H. Cho, H. J. Kim, C. Lee, D. Lymberopoulos, J. Yoon, W. Han, and J. T. Moon, *Jpn. J. Appl. Phys.* 48, 08HD01 (**2009**).
24. D. J. Economou, *J. Phys. D: Appl. Phys.* 47, 303001 (**2014**).
25. H. V. Jansen, M. J. de Boer, S. Unnikrishnan, M. C. Louwerse, and M. C. Elwenspoek, *J. Micromech. Microeng.* 19, 033001 (**2009**).

Received: 17 August 2014. Accepted: 18 March 2015.